Modelling and Control Techniques of an Active Vibration Isolation System

Thorsten Müller*, Stefan Hurlebaus*, Uwe Stöbener**, Lothar Gaul*
*Institute A of Mechanics, University of Stuttgart, Pfaffenwaldring 9, 70550 Stuttgart, Germany
s.hurlebaus@mecha.uni-stuttgart.de
**Halcyonics GmbH, Tuchmacherweg 12, 37079 Göttingen, Germany

ABSTRACT

In the field of high-resolution measurement and manufacturing, effective anti-vibration measures are required to obtain precise and repeatable results. This is particularly true for experiments or processes where the typical amplitudes of the ambient vibration and the dimensions of the investigated or manufactured structures fall in the same range, e.g. submicron semiconductor production, holographic interferometry, confocal optical imaging, and scanning probe microscopy. In the active vibration isolation system examined, signals are acquired by extremely sensitive vibration detectors, and the vibration is reduced using either local analog feedback control or digital model-based control to drive electrodynamic actuators.
This papers deals with the modelling and control techniques of such an active vibration isolation system. The modelling, parameter identification, and model updating procedure are described. The experimental setup for testing such an anti-vibration system is described, and the measured transmissibility curves for the passive and active system being driven by local analog feedback controllers are provided. Finally, the simulated transmissibility curves of the passive system and the active system using a decentralized digital loop shaping controller and a centralized model based controller are given and the results are discussed.

1 Introduction

Isolating a piece of delicate equipment from the vibration of a base structure is of practical importance in a number of engineering fields. For instance, in industry and research the quest for tighter production tolerance and higher resolution places stringent requirements on the environment. In the majority of cases, the base is flexible and vibrates with an unpredictable waveform which has a broadband spectrum. The active isolation of vibration sensitive equipment from a vibrating base is studied in this paper. Passive anti-vibration mounts are widely used to support the equipment and protect it from severe base vibration. However, conventional passive mounts suffer from the inherent trade-off between poor high frequency isolation and amplification of vibration at the fundamental mounted resonance frequency. Generally the best isolation performance is achieved by using an active system in combination with a passive mount, where the fundamental resonance can be actively controlled without reducing the high frequency performance.

Fuller et al. [2] gives a deep understanding and background in the field of active isolation of vibrations. Various control strategies are discussed including feedforward and feedback concepts for systems under periodic as well as random vibrations.

Stöbener and Gaul [10] and Hurlebaus [5] modeled a piezoelectric stack actuator with finite elements in order to describe the behavior of a one degree of freedom vibration isolation system. To validate the FE formulation and to evaluate the performance of the vibration isolation system with the stack actuator, they designed and tested an experimental setup. They examined both feedforward control as well as feedback control techniques to enhance the isolation effect. Huang et al. [4] presented a theoretical and experimental investigation of an active vibration isolation system. In that study, a decentralized velocity feedback control was employed, whereby each electrodynamic actuator is operated independently by feeding back the absolute equipment velocity at the same location. They obtained good control and robust stability both experimentally and theoretically for the multichannel control systems.

Preumont et al. [6, 7] compared the force feedback and acceleration feedback implementation of a sky hook damper used to isolate a flexible structure from a disturbance source. They showed that the use of a force sensor always produces alternating poles and zeros in the open-loop transfer function between the force actuator and the force sensor, which guarantees stability of the closed loop. On the contrary, the acceleration feedback produces alternating poles and zeros only when the flexible structure is stiff compared to the isolation system.

Riebe and Ulbrich [8] presented the model of a parallel robot with six degrees of freedom for the use in real time computation of the inverse dynamic. They modeled the frictional behavior, and the parameters describing the friction model are identified and optimized. Furthermore, they presented a comparison between the measured and the simulated actuation forces.

This paper investigates a four mount six degrees of freedom system for active vibration isolation and suppression. The system itself is based on a decentralized analog velocity feedback controller. Fig. 1 depicts the examined active vibration isolation system. The experimental setup for measuring the transmissibility curve is described in the first section. Then the system is modeled using the balance of linear and angular momentum. This leads to the governing equations of motion. The parameters necessary to describe the system's behavior are identified, and the parameters are then optimized by model updating. A comparison between the updated model and the measurements show good agreement. Next, some control concepts are described, and the simulated transmissibility curves are presented. The simulation show that the global digital control technique has great potential for enhancing the isolation performance of the system.

Figure 1: Active vibration isolation system.

2 Experimental Setup

This section describes the experimental setup for measuring the performance of the isolation systems. As shown in Fig. 2, the setup consists of a heavy base plate which is suspended on six springs. In order to minimize the interaction between the vibration isolation system and the spring-mass-system of the experimental setup, the mass of the base plate (2 t) is chosen to be much larger than the mass of the vibration isolation system (30 kg). The isolation performance can be determined by constructing a transmissibility curve. Transmissibility is simply the response of the isolation system divided by the excitation (in the frequency domain), where the response and excitation have been measured with accelerometers. The excitation of the base plate is realized using a conventional loudspeaker which is connected to the base plate via a stinger. The output from the function generator is first amplified using a conventional HIFI amplifier before being used to drive the loudspeaker. The rigid body eigenfrequencies of the spring supported base plate are between 1.44 and 2.88 Hz. Fig. 3 depicts the measured transmissibility curves for the passive and active isolation systems, respectively. Here, the active system is realized using a decentralized analog feedback controller. It is seen that almost over the entire frequency range a significant reduction in the transmissibillity curve is obtained using the active system. At frequencies above 40 Hz, noise appears in both curves. This is due to the dynamic behavior of the actuators.

3 Modelling

The modeling of the vibration isolation system is restricted to three degrees of freedom. The possible movement is a translation in vertical direction (z-direction), as well as rotation about the other axes (x- and y-axis). Further assumptions are made for the modeling of the system:

1. The displacement is small compared to system dimensions.
2. The spring force is linear around the working point.

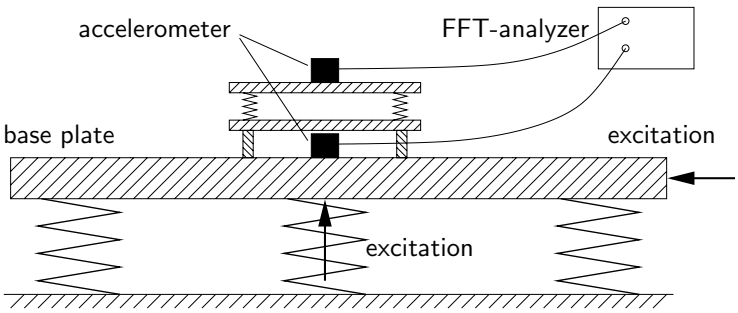

Figure 2: Experimental setup for testing of the active vibration isolation system.

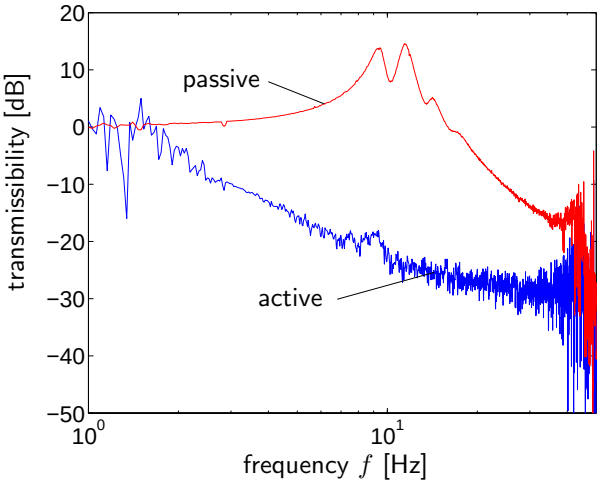

Figure 3: Measured vertical transmissibility curves for the passive and active vibration isolation system.

3. The upper plate on the vibration isolation system is a rigid body.

During operation, the vibration amplitudes of the vibration isolation system are smaller than 1 to 2 mm. Since the important system dimensions, $L_1 = 348\,\text{mm}$, $L_2 = 300\,\text{mm}$, $a = 55\,\text{mm}$ are large by comparison assumption (1) is justified (Fig. 4).

3.1 Coordinate System

In order to describe the behavior of the vibration isolation system, it is necessary to introduce a set of coordinate systems and the relationships among the various coordinates. In the upper left corner of Fig. 4, the inertial coordinate system is shown. The coordinates d_i represent the excitation displacement of the legs of the vibration isolation system, and the coordinates z_i represent the absolute displacement of the points on the upper plate where the springs are attached. It is assumed that z_i and d_i are zero at equilibrium. The coordinates $d_i^\star$ and $z_i^\star$ represent excitation displacement of the system and the absolute displacement of the upper plate, respectively, at the locations of the actuators. The coordinates denoted with the subscript c characterize a space-fixed coordinate system, whose origin is at the center of mass of the piece of equipment being isolated. It is assumed that the z_c-axis intersects the centroid of the upper plate, so that symmetry can be assumed. The coordinates z_c, $\varphi_{\mathrm{c}x}$, and $\varphi_{\mathrm{c}y}$ fully describe the state of the system and are taken as the generalized coordinates.

The relationship between the generalized coordinate z_c and the absolute displacements z_i can be stated as

$$z_\mathrm{c} = \frac{1}{4}(z_1 + z_2 + z_3 + z_4)\,. \tag{1}$$

Assuming small angles $\varphi_{\mathrm{c}x}, \varphi_{\mathrm{c}y} << 1$ one obtains

$$\varphi_{\mathrm{c}x} = \frac{1}{2L_2}[(z_4 - z_1) + (z_3 - z_2)] \tag{2}$$

$$\varphi_{\mathrm{c}y} = \frac{1}{2L_1}[(z_1 - z_2) + (z_4 - z_3)]\,. \tag{3}$$

Under the assumption of small displacements the absolute displacement are constrained by

$$z_1 + z_3 = z_4 + z_2\,. \tag{4}$$

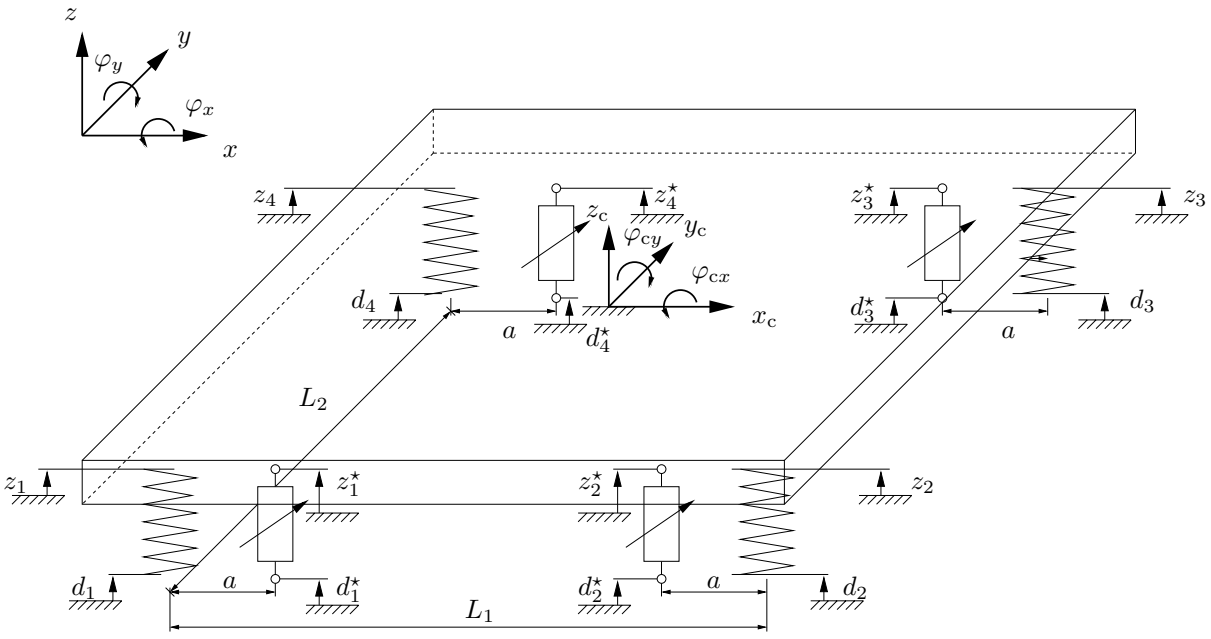

Figure 4: Coordinate systems.

Solving Equations (1) to (4), in terms of z_i, $i = 1, ..., 4$ gives

$$z_1 = z_c - \frac{1}{2}\varphi_{cx}L_2 + \frac{1}{2}\varphi_{cy}L_1 \tag{5}$$

$$z_2 = z_c - \frac{1}{2}\varphi_{cx}L_2 - \frac{1}{2}\varphi_{cy}L_1 \tag{6}$$

$$z_3 = z_c + \frac{1}{2}\varphi_{cx}L_2 - \frac{1}{2}\varphi_{cy}L_1 \tag{7}$$

$$z_4 = z_c + \frac{1}{2}\varphi_{cy}L_1 + \frac{1}{2}\varphi_{cx}L_2\,. \tag{8}$$

The absolute displacement z_i and $z_i^\star$ are related as

$$z_1^\star = z_1\left(1 - \frac{a}{L_1}\right) + z_2\frac{a}{L_1} \tag{9}$$

$$z_2^\star = z_1\frac{a}{L_1} + z_2\left(1 - \frac{a}{L_1}\right) \tag{10}$$

$$z_3^\star = z_4\frac{a}{L_1} + z_3\left(1 - \frac{a}{L_1}\right) \tag{11}$$

$$z_4^\star = z_4\left(1 - \frac{a}{L_1}\right) + z_3\frac{a}{L_1}\,. \tag{12}$$

An identical set of relations relate the displacements $d_i^\star$ and d_i on the lower plate, which is also modeled as rigid body.

3.2 Free Body Diagram

As previous stated only the forces required to describe the dynamics of the systems are considered here. The static weighting force of the upper plate is therefore neglected. The constitutive equation for the dynamic forces f_i can be written as

$$f_i = -k(z_i - d_i)\,. \tag{13}$$

The equations for the actuator forces F_i are

$$F_i = -k_a(z_i^\star - d_i^\star) - D_a(\dot{z}_i^\star - \dot{d}_i^\star) + u_i, \qquad i = 1, \ldots, 4 \tag{14}$$

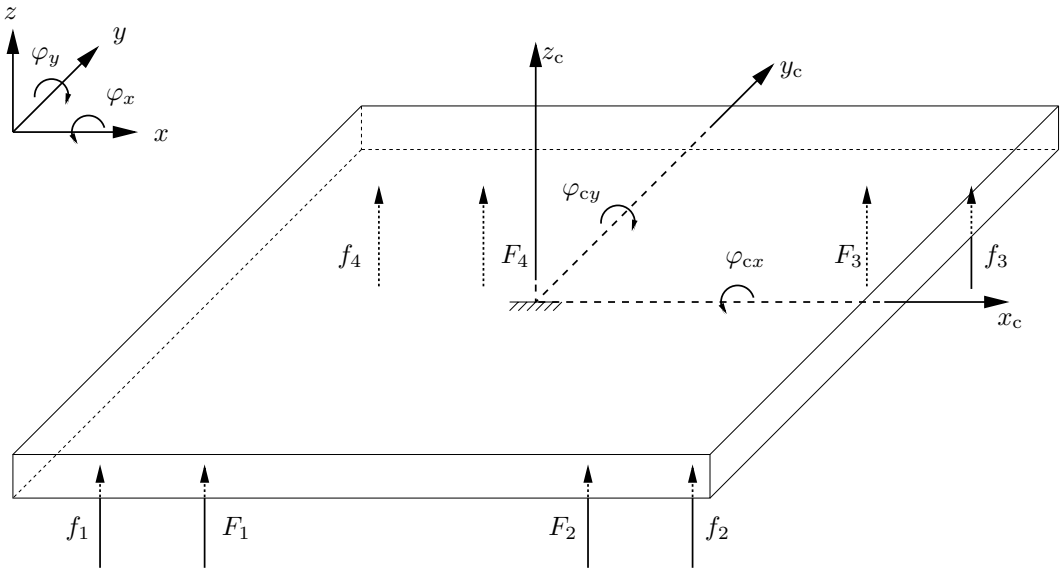

Figure 5: Free body diagram.

where k_a is the actuator spring constant, D_a is the damping parameter, and u_i is the actuator excitation force. Note, that the actuator forces can act in positive as well as in negative direction.

3.3 Balance of Linear and Angular Momentum

Applying the balance of linear momentum to the upper plate gives

$$m\ddot{z}_c = \sum_{i=1}^{4}(f_i + F_i)\,, \tag{15}$$

where m is the plate mass. Substituting Equations (13) and (14) into (15) gives

$$m\ddot{z}_c = \sum_{i=1}^{4}\left[-k(z_i - d_i) - k_a(z_i^\star - d_i^\star) - D_a(\dot{z}_i^\star - \dot{d}_i^\star) + u_i\right]. \tag{16}$$

The balance of angular momentum with respect to the center of mass of the upper plate gives

$$\mathbf{M}^c = \mathbf{J}^c\ddot{\boldsymbol{\varphi}} \tag{17}$$

with

$$\mathbf{M}^c = \begin{pmatrix} M_x^c \\ M_y^c \end{pmatrix}, \qquad \mathbf{J}^c = \begin{bmatrix} J_{xx} & 0 \\ 0 & J_{yy} \end{bmatrix}, \qquad \text{and} \qquad \boldsymbol{\varphi} = \begin{pmatrix} \varphi_{cx} \\ \varphi_{cy} \end{pmatrix}. \tag{18}$$

Hence $\mathbf{M}^c$ is the vector of moments with respect to the center of mass, $\mathbf{J}^c$ is the moment of inertia with respect to the center of mass, and $\boldsymbol{\varphi}$ is the corresponding rotational vector. The moments can be obtained by considering the free body diagram, Fig. 5,

$$\begin{aligned} M_x^c &= -\frac{L_2}{2}(f_1 + f_2 + F_1 + F_2) + \frac{L_2}{2}(f_3 + f_4 + F_3 + F_4) \\ M_y^c &= \frac{L_1}{2}(f_1 + f_4) - \frac{L_1}{2}(f_2 + f_3) + \left(\frac{L_1}{2} - a\right)(F_1 + F_4) - \left(\frac{L_1}{2} - a\right)(F_2 + F_3) \end{aligned} \tag{19}$$

By implementing the relations for the forces equations (13) and (14) into the moment equation (19) and subsequently implementing these into the equation of angular momentum (17) leads together with the balance of linear momentum (16) to the governing equation of motion

$$\mathbf{M}\,\ddot{\tilde{\mathbf{x}}} + \mathbf{D}\,\dot{\tilde{\mathbf{x}}} + \mathbf{K}\,\tilde{\mathbf{x}} = \mathbf{F_u}\,\mathbf{u} + \mathbf{F_d}\,\mathbf{d} + \mathbf{F_{dd}}\,\dot{\mathbf{d}}\,, \tag{20}$$

where

$$\mathbf{M} = \begin{bmatrix} m & 0 & 0 \\ 0 & J_{xx} & 0 \\ 0 & 0 & J_{yy} \end{bmatrix} \tag{21}$$

is the mass matrix,

$$\mathbf{D} = \begin{bmatrix} 4D_\mathrm{a} & 0 & 0 \\ 0 & D_\mathrm{a}L_2^2 & 0 \\ 0 & 0 & D_\mathrm{a}(L_1^2 - 4L_1a + 4a^2) \end{bmatrix} \tag{22}$$

is the damping matix

$$\mathbf{K} = \begin{bmatrix} 4(k+k_\mathrm{a}) & 0 & 0 \\ 0 & L_2^2(k+k_\mathrm{a}) & 0 \\ 0 & 0 & L_1^2k + (-4L_1a + 4a^2 + L_1^2)k_\mathrm{a} \end{bmatrix} \tag{23}$$

is the stiffness matrix,

$$\mathbf{F_u} = \begin{bmatrix} 1 & 1 & 1 & 1 \\ -\frac{1}{2}L_2 & -\frac{1}{2}L_2 & \frac{1}{2}L_2 & \frac{1}{2}L_2 \\ -a + \frac{1}{2}L_1 & a - \frac{1}{2}L_1 & a - \frac{1}{2}L_1 & -a + \frac{1}{2}L_1 \end{bmatrix} \tag{24}$$

is the control matrix, and the matrices

$$\mathbf{F_d} = \begin{bmatrix} k+k_\mathrm{a} & k+k_\mathrm{a} \\ -\frac{1}{2}L_2(k+k_\mathrm{a}) & -\frac{1}{2}L_2(k+k_\mathrm{a}) \\ \frac{1}{2L_1}(-4L_1k_\mathrm{a}a + 4k_\mathrm{a}a^2 + k_\mathrm{a}L_1^2 + L_1^2k) & \frac{1}{2L_1}(-k_\mathrm{a}L_1^2 + 4L_1k_\mathrm{a}a - L_1^2k - 4k_\mathrm{a}a^2) \\ k+k_\mathrm{a} & k+k_\mathrm{a} \\ \frac{1}{2}L_2(k+k_\mathrm{a}) & \frac{1}{2}L_2(k+k_\mathrm{a}) \\ \frac{1}{2L_1}(4L_1k_\mathrm{a}a - k_\mathrm{a}L_1^2 - L_1^2k - 4k_\mathrm{a}a^2) & \frac{1}{2L_1}(-4L_1k_\mathrm{a}a + 4k_\mathrm{a}a^2 + k_\mathrm{a}L_1^2 + L_1^2k) \end{bmatrix} \tag{25}$$

and

$$\mathbf{F_{dd}} = \begin{bmatrix} D_\mathrm{a} & D_\mathrm{a} & D_\mathrm{a} & D_\mathrm{a} \\ -\frac{1}{2}L_2D_\mathrm{a} & -\frac{1}{2}L_2D_\mathrm{a} & \frac{1}{2}L_2D_\mathrm{a} & \frac{1}{2}L_2D_\mathrm{a} \\ \frac{D_\mathrm{a}}{2L_1}(L_1^2 + 4a^2 - 4L_1a) & \frac{D_\mathrm{a}}{2L_1}(4L_1a - 4a^2 - L_1^2) & \frac{D_\mathrm{a}}{2L_1}(4L_1a - 4a^2 - L_1^2) & \frac{D_\mathrm{a}}{2L_1}(L_1^2 + 4a^2 - 4L_1a) \end{bmatrix} \tag{26}$$

describe the disturbance of the upper plate. The vector $\tilde{\mathbf{x}} = [z_\mathrm{c}, \varphi_{cx}, \varphi_{cy}]^\mathrm{T}$ represents the general coordinates, $\mathbf{u} = [u_1, u_2, u_3, u_4]^\mathrm{T}$ is the control input, and $\mathbf{d} = [d_1, d_2, d_3, d_4]^\mathrm{T}$ is the vector of the displacement disturbances which are introduced at the lower plate.

4 Parameter Identification

This section describes the identification of the system parameters, e.g. the geometry, mass, spring characteristic, electrodynamic actuator characteristics and the moments of inertia. Without well-identified parameters, it is impossible to simulate the system, and therefore new control techniques cannot be examined.

4.1 Geometry and Mass

The side length of the upper square plate is 404 mm, and its thickness is 25 mm. The distance between the springs in x- and y-directions are $L_1 = 348$ mm and $L_2 = 300$ mm, respectively, and the distance between the actuators and the springs is $a = 55$ mm.
The mass of the isolation system consists of the mass of upper plate, the mass of the sensor-actuator units and one half of the spring masses which support the upper plate. The total mass of these parts is $m_\mathrm{sys} = 19.274$ kg.

4.2 Spring Characteristic

For the determination of the spring characteristic, a spring is loaded by different masses, and the applied force is plotted as a function of displacement. The force-displacement characteristic is depicted in Fig. 6 along with a linear interpolation and a spline curve fit to the data. It can be seen that the relation between the restoring force and the displacement is nonlinear. The dependency between the spring characteristic and the force is calculated from the linear and spline interpolation and is depicted in Fig. 7. Refering to Fig. 7, an empirical logarithmic relation has been determined which describes the spring constant vs. force relationship necessary for the working point linearization.

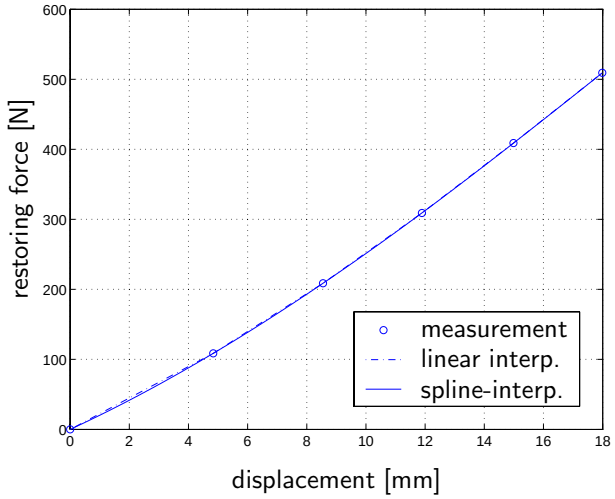

Figure 6: Force-displacement relation.

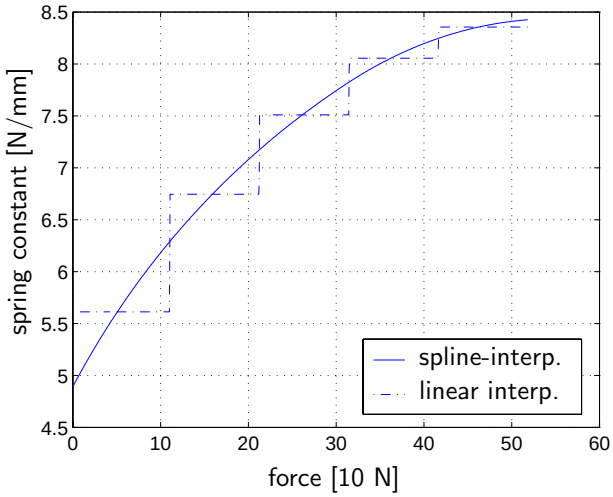

Figure 7: Spring constant-force relation.

4.3 Electrodynamic Actuator

The electrodynamic actuator has its own dynamics. The experimental setup for determination of the actuator parameter is depicted in Fig. 8. In order to obtain the transfer function for the actuator, the actuator is driven using a random signal. The output is measured by a force cell which is placed between the actuator rod and the mass. The measured transfer function is shown in Fig. 9, where the amplitude is given by the ratio of the force to the applied voltage.

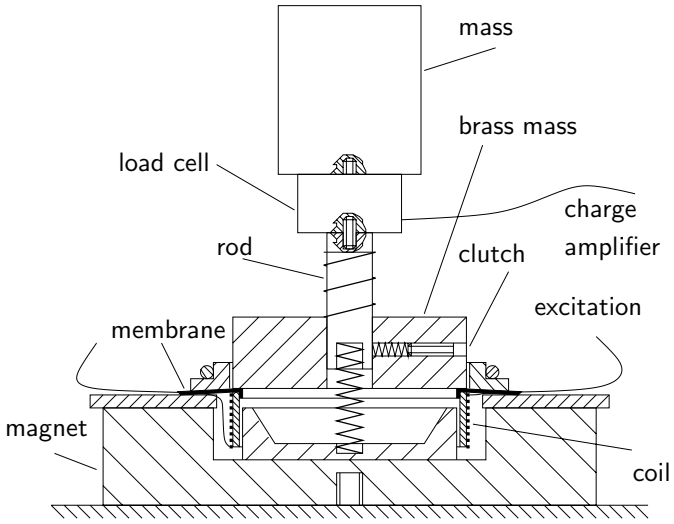

Figure 8: Experimental setup for the determination of the actuator parameters.

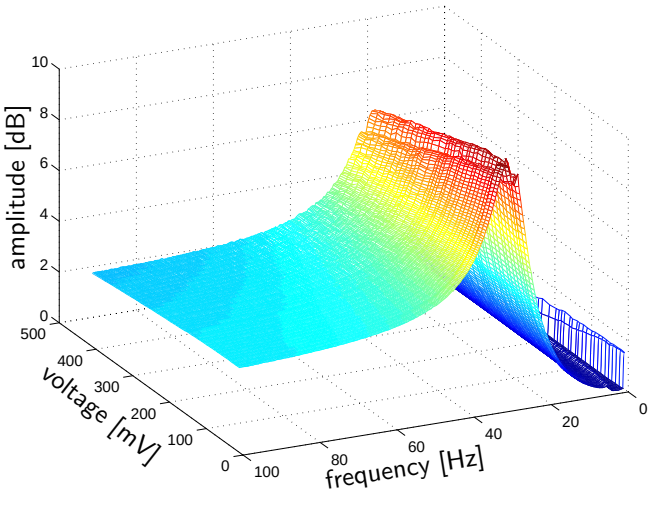

Figure 9: Transfer function of the actuator.

In order to identify the parameters, a model of the actuator is required. The model is shown in Fig. 10, where F_{a} represents

the actuator force, m_a is the entire mass of the moving parts, U_a is the applied voltage, k_a is the spring stiffness, and d_a is the corresponding damping parameter [6]. A reaction mass is attached to a current-carrying coil moving in a magnetic

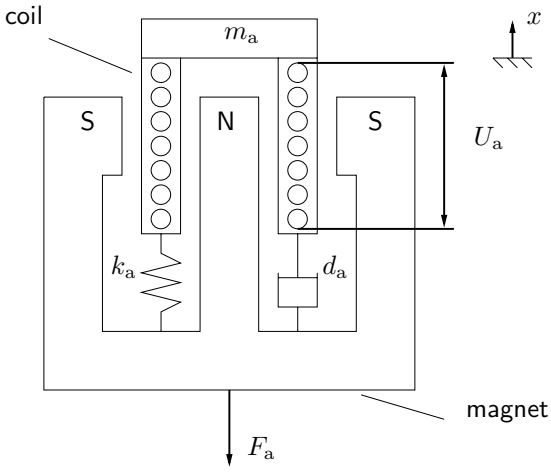

Figure 10: Model of the electrodynamic actuator.

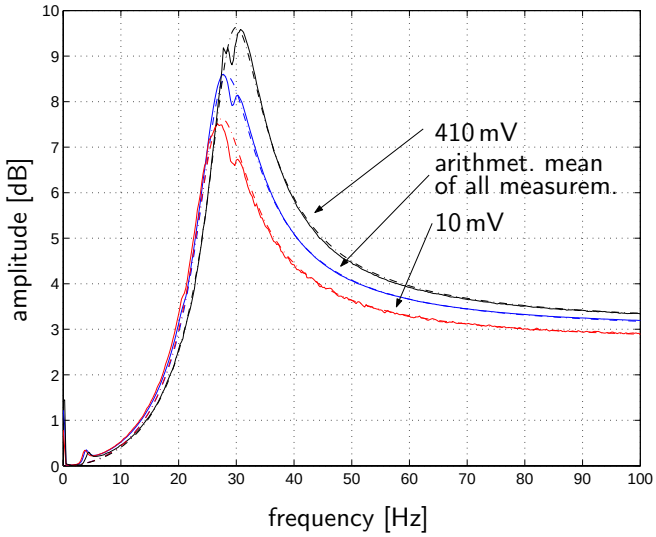

Figure 11: Output of an electrodynamic actuator.

field created by a permanent magnet. The moving part is attached to the chassis by a spring k_a and a damper d_a (Fig. 10). The current in the coil is governed by

$$Ri + \frac{\mathrm{d}i}{\mathrm{d}t}L = U_\mathrm{a} - C_1\dot{x}\,, \tag{27}$$

where R is the resistance and L is the inductance of the coil, and $-C_1\dot{x}$ is the back electromotive voltage due to motion. The equation of motion of the moving part is

$$m_\mathrm{a}\ddot{x} + d_\mathrm{a}\dot{x} + k_\mathrm{a}x = F \tag{28}$$

where F is the electromagnetic force. The force is proportional to the current in the coil according to the relationship

$$F = C_2 i\,. \tag{29}$$

Transforming Equations (27) to (29) into the Laplace domain and combining them yields

$$\left(m_\mathrm{a}s^2 + \left(d_\mathrm{a} + \frac{C_1C_2}{R+sL}\right)s + K\right)x = \frac{C_2}{R+sL}U_\mathrm{a},\,. \tag{30}$$

The balance of linear momentum leads to $F_\mathrm{a} = -m_\mathrm{a}\ddot{x}$, or in the Laplace domain, $F_\mathrm{a} = -m_\mathrm{a}s^2x$. Combining with Equation (30), one obtains the transfer function between the force F_a and the voltage U_a

$$\frac{F_\mathrm{a}}{U_\mathrm{a}} = \frac{-m_\mathrm{a}C_2s^2}{m_\mathrm{a}Ls^3 + (Rm_\mathrm{a} + d_\mathrm{a}L)\,s^2 + (d_\mathrm{a}R + C_1C_2 + k_\mathrm{a}L)\,s + k_\mathrm{a}R}\,. \tag{31}$$

In order to identify the parameters, the model has to be updated to the measured transfer function. Fig. 11 shows the modelled transfer function (dashed lines) as well as the measured transfer functions (solid lines). Neglecting the inductance of the coil, using the measured resistance $R = 6.34\,\Omega$, the moving mass $m_\mathrm{a} = 342.75\,\mathrm{g}$ and assuming $C_1 = 0$, one obtains for the case of applied arithmetic mean voltage the remaining parameters: $k_\mathrm{a} = 10.2$ N/mm, $d_\mathrm{a} = 20.7$ Ns/m, $C_2 = 1.47\,10^3$ N/mA.

4.4 Moments of Inertia

For identification of the moment of inertia the upper part of the system is supported by the outer springs only. Then the eigenfrequencies of the system are determined. The eigenfrequency in the vertical direction is $\omega_{cz} = 6.16$ Hz, and the rotational eigenfrequencies with respect to the $x-$ and y-axes are $\omega_{\varphi_{cx}} = 7.28$ Hz and $\omega_{\varphi_{cy}} = 9.91$ Hz, respectively. Based on the homogeneous differential equation of motion (20) with $k_\mathrm{a} = 0$ and $D_\mathrm{a} = 0$ (the system is not connected to the actuators), the spring stiffness is $k = \omega_{cz}^2 m_\mathrm{sys}/4 = 7282$ N/m and the moment of inertias are $J_{xx} = L_2^2 k/\omega_{\varphi_{cx}}^2 = 0.313$ kgm^2 and $J_{yy} = L_1^2 k/\omega_{\varphi_{cy}}^2 = 0.228$ kgm^2.

5 Model Updating

The described model is updated by measurements. An impact hammer is used to apply impulsive excitation at the location of the $z_i^\star$-coordinates (actuator attachment points on the upper plate), and accelerometers are used to measure the resultant motion at the z_i-coordinate locations (spring attachment points on the upper plate). The signals are processed using an FFT analyzer, and the measured force displacement transfer functions are compared with that obtained using the physical model. 16 different transfer functions are constructed by forming the ratio of u_i, $i = 1, ..., 4$ to z_j, $j = 1, ..., 4$. Using Equations (1), (2), and (3), the generalized coordinates can be expressed in terms of z_i, $i = 1, ..., 4$. Using the balance of linear and angular momentum, Eqs. (16) and (17), respectively, Equation (20) can be expressed in terms of z_i. Hence all matrices have the dimension 3 x 4, since the balance of linear and angular momentum give three equations as functions of four coordinates. A fourth condition is obtained using the constraint (Equation (4)). The resultant system can be described by the equation

$$\mathbf{M}^\star \begin{bmatrix} \ddot{z}_1 \\ \ddot{z}_2 \\ \ddot{z}_3 \\ \ddot{z}_4 \end{bmatrix} + \mathbf{D}^\star \begin{bmatrix} \dot{z}_1 \\ \dot{z}_2 \\ \dot{z}_3 \\ \dot{z}_4 \end{bmatrix} + \mathbf{K}^\star \begin{bmatrix} z_1 \\ z_2 \\ z_3 \\ z_4 \end{bmatrix} = \mathbf{F}_\mathbf{u}^\star \begin{bmatrix} u_1 \\ u_2 \\ u_3 \\ u_4 \end{bmatrix} + \mathbf{F}_\mathbf{d}^\star \, \mathbf{d} + \mathbf{F}_\mathbf{dd}^\star \, \dot{\mathbf{d}} \, . \tag{32}$$

Neglecting the disturbance terms and assuming zero initial conditions, Equation (32) is transformed into Laplace domain

$$\left(s^2\mathbf{M}^\star + s\mathbf{D}^\star + \mathbf{K}^\star\right) \begin{bmatrix} Z_1 \\ Z_2 \\ Z_3 \\ Z_4 \end{bmatrix} = \mathbf{F}_\mathbf{u}^\star \begin{bmatrix} U_1 \\ U_2 \\ U_3 \\ U_4 \end{bmatrix} \, . \tag{33}$$

Equation (33) can be recast in the form

$$\begin{bmatrix} Z_1 \\ Z_2 \\ Z_3 \\ Z_4 \end{bmatrix} = \begin{bmatrix} g_a & g_b & g_c & g_d \\ g_b & g_a & g_d & g_c \\ g_c & g_d & g_a & g_b \\ g_d & g_c & g_b & g_a \end{bmatrix} \begin{bmatrix} U_1 \\ U_2 \\ U_3 \\ U_4 \end{bmatrix} = \mathbf{G}(s) \begin{bmatrix} U_1 \\ U_2 \\ U_3 \\ U_4 \end{bmatrix} \, , \tag{34}$$

where $\mathbf{G}(s)$ is the transfer matrix. Since the physical system is symmetric, the transfer matrix is symmetric as well. In this research, the response function method (RFM) is used for model updating. An exhaustive description of updating techniques is given in Ewins [3]. The parameters used for the updating procedure are the spring constant of the system, k, the spring constant of the actuator, k_a, and the damping parameter of the actuator, D_a. It turns out that the measured response functions and the updated response function fit well for values of $k = 6958$ N/m, $k_\mathrm{a} = 8902$ N/m, and $D_\mathrm{a} = 20$ Ns/m.

As an example, Fig. 12 shows the amplitude and phase frequency response functions of the measured and the modeled updated transfer function $\mathbf{G}(s)$. Agreement between the experimental and model amplitude and phase characteristics is good. This is an indication that the parameter errors and the structural errors of the model are small [3], and therefore the model can be used in further considerations.

6 Control Techniques

6.1 State Variable Approach

Neglecting the disturbance and assuming that the mass matrix $\mathbf{M}$ is of full rank ($m \neq 0$, $J_{xx} \neq 0$, $J_{yy} \neq 0$) one can transfer the governing equation of motion (20) into the state-space representation,

$$\underbrace{\frac{\mathrm{d}}{\mathrm{d}t} \begin{bmatrix} \tilde{\mathbf{x}} \\ \dot{\tilde{\mathbf{x}}} \end{bmatrix}}_{\dot{\mathbf{x}}} = \underbrace{\begin{bmatrix} \mathbf{0} & \mathbf{I} \\ -\mathbf{M}^{-1}\mathbf{K} & -\mathbf{M}^{-1}\mathbf{D} \end{bmatrix}}_{\mathbf{A}} \underbrace{\begin{bmatrix} \tilde{\mathbf{x}} \\ \dot{\tilde{\mathbf{x}}} \end{bmatrix}}_{\mathbf{x}} + \underbrace{\begin{bmatrix} \mathbf{0} \\ \mathbf{F_u} \end{bmatrix}}_{\mathbf{B}} \mathbf{u} \, , \tag{35}$$

where the state vector $\mathbf{x}$ contains not only the generalized coordinates z_c, $\varphi_{\mathrm{c}x}$ und $\varphi_{\mathrm{c}y}$, but also their derivatives with respect to time. $\mathbf{A}$ is the system matrix, and $\mathbf{B}$ is the control matrix.

The output of the system can be described by using Equations (1) to (3) in order to relate the measured accelerations to the generalized coordinates. Therefore the system output is

$$\mathbf{y} = [\ddot{z}_\mathrm{c}, \, \ddot{\varphi}_{\mathrm{c}x}, \, \ddot{\varphi}_{\mathrm{c}y}]^\mathrm{T} = \underbrace{\left[-\mathbf{M}^{-1}\mathbf{K} \, -\mathbf{M}^{-1}\mathbf{D}\right]}_{\mathbf{C}} \mathbf{x} + \underbrace{\mathbf{F_u}}_{\mathbf{D}} \mathbf{u} \, , \tag{36}$$

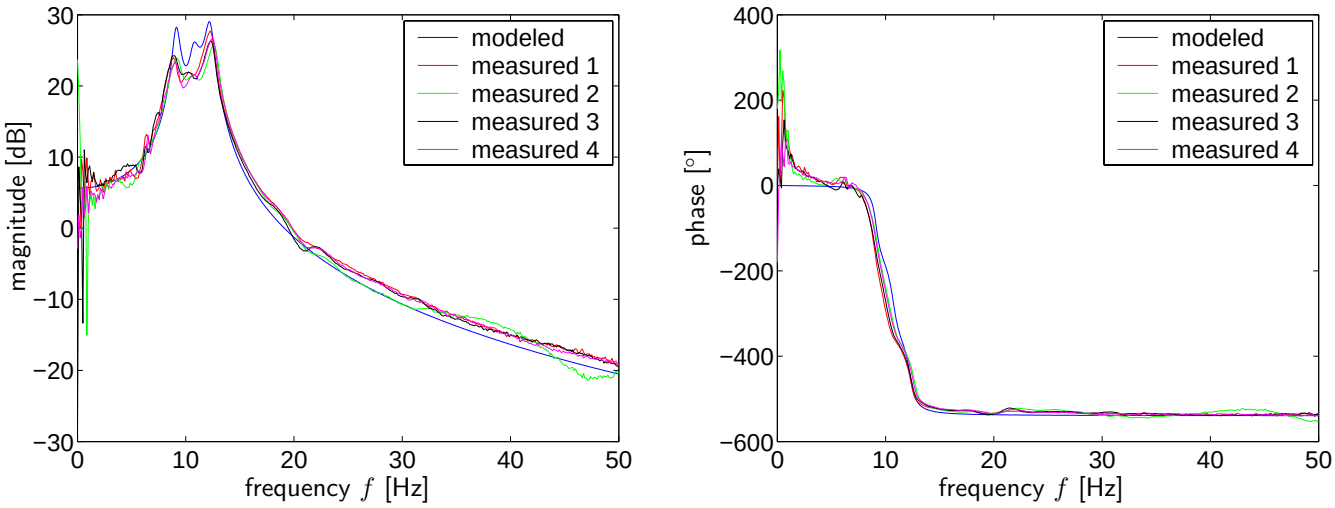

Figure 12: Amplitude and phase frequency response function.

where $\mathbf{C}$ is the output matrix and $\mathbf{D}$ is the feedthrough matrix.

6.2 Single Input Single Output (SISO)

6.2.1 Transfer Function

The transfer matrix $\mathbf{G}(s)$ can be obtained either by Laplace transformation of the governing equation of motion and solving the subsequent linear set of equations or by using the state approach representation,

$$\mathbf{G}(s) = \mathbf{C}\left(s\mathbf{I} - \mathbf{A}\right)^{-1}\mathbf{B} + \mathbf{D}\,. \tag{37}$$

6.2.2 Loop Shaping

In the following, a decentralized control concept is realized, in which each actuator is controlled by its corresponding sensor.

In section 5, the construction of the transfer matrix from the system inputs, u_i, and outputs, z_i, is described. Analogously, it is possible to construct the transfer matrix from the $z_i^\star$-coordinates, which locate the sensors, and the system's input u_i. The transfer matrix $\mathbf{G}^\star_{\mathrm{sys}}(s)$ in this case is

$$\begin{bmatrix} Z_1^\star \\ Z_2^\star \\ Z_3^\star \\ Z_4^\star \end{bmatrix} = \mathbf{G}^\star_{\mathrm{sys}}(s) \begin{bmatrix} U_1 \\ U_2 \\ U_3 \\ U_4 \end{bmatrix}\,. \tag{38}$$

By differentiating twice with respect to time, which is just the multiplication with the factor s^2, one obtains the required transfer matrix of the system input to the system output as

$$s^2 \begin{bmatrix} Z_1^\star \\ Z_2^\star \\ Z_3^\star \\ Z_4^\star \end{bmatrix} = \begin{bmatrix} Y_1 \\ Y_2 \\ Y_3 \\ Y_4 \end{bmatrix} = \underbrace{s^2\,\mathbf{G}^\star_{\mathrm{sys}}(s)}_{\mathbf{G}_{\mathrm{sys}}(s)} \begin{bmatrix} U_1 \\ U_2 \\ U_3 \\ U_4 \end{bmatrix}\,. \tag{39}$$

For this control concept, only the diagonal terms of $\mathbf{G}_{\mathrm{sys}}(s)$ are considered, since each actuator, which is collocated to one sensor, responds primarily to inputs from its corresponding sensor. Fig. 13 shows the simulated transmissibility curves for the passive system and loop shaping controller cases. In this context, transmissibility is understood as the displacement ratio $4z_c/(d_1 + d_2 + d_3 + d_4)$. It can be seen that by using the feedback controller, a significant improvement in the transmissibility curve is obtained over a broad frequency range.

6.3 Multiple Input Multiple Output (MIMO)

6.3.1 Controllability and Observability

It is necessary to prove the controllability and observability before a controller is designed. A linear system $\dot{\mathbf{x}} = \mathbf{A}\,\mathbf{x} + \mathbf{B}\,\mathbf{u}$, $\mathbf{x} \in R^n$ is controllable if the rank of the controllability matrix $\mathbf{S}$ is n,

$$\operatorname{rank}\mathbf{S} \;=\; \operatorname{rank}\left[\mathbf{B}\;\mathbf{AB}\;\ldots\;\mathbf{A}^{n-1}\mathbf{B}\right] \;=\; n\,. \tag{40}$$

Since this condition is already fulfilled by the matrix $[\mathbf{B}\;\mathbf{AB}]$, the system is controllable. Similarly, the condition for observability states that the system $\dot{\mathbf{x}} = \mathbf{A}\,\mathbf{x}$, $\mathbf{y} = \mathbf{C}\,\mathbf{x}$, $\mathbf{x} \in R^n$ is observable if the observability matrix $\mathbf{P}^T$ has the rank n,

$$\operatorname{rank}\mathbf{P}^T = \operatorname{rank}\begin{bmatrix}\mathbf{C}\\ \mathbf{CA}\\ \ldots\\ \mathbf{CA}^{n-1}\end{bmatrix} \;=\; n\,. \tag{41}$$

This condition is fulfilled as well.

6.3.2 State Feedback with Observer

It is not always the case that all state variables can be calculated directly from the outputs. Therefore a state estimator or observer strategy has been developed to estimate the state variables from a limited number of observations. The estimated states $\dot{\hat{\mathbf{x}}}$ would thus be governed using the system equation in the state variable approach (35) and (36)

$$\dot{\hat{\mathbf{x}}} \;=\; \mathbf{F}\,\hat{\mathbf{x}} + \mathbf{E}\,\mathbf{y} + \mathbf{L}\,\mathbf{u} \tag{42}$$

$$\hat{\mathbf{y}} \;=\; \mathbf{C}\,\hat{\mathbf{x}} + \mathbf{D}\,\mathbf{u}\,. \tag{43}$$

The 'correction matrix' $\mathbf{E}$ has to be chosen in a way that the estimated error $\mathbf{e}(t) = \mathbf{x}(t) - \hat{\mathbf{x}}(t)$ approaches zero for $t \to \infty$. The dynamic equation of the error becomes

$$\dot{\mathbf{e}} = \dot{\mathbf{x}} - \dot{\hat{\mathbf{x}}} = (\mathbf{A} - \mathbf{EC})\;\mathbf{x} - \mathbf{F}\,\hat{\mathbf{x}} + (\mathbf{B} - \mathbf{ED})\;\mathbf{u} - \mathbf{L}\,\mathbf{u}\,. \tag{44}$$

Choosing $\mathbf{F} = (\mathbf{A} - \mathbf{EC})$ and $\mathbf{L} = (\mathbf{B} - \mathbf{ED})$, then the estimated error approaches zero for $t \to \infty$ if the eigenvalues of $\mathbf{F} = (\mathbf{A} - \mathbf{EC})$ are in the left half plane. Using the principle of separation, the poles of the observability matrix can be chosen independently from those in the state feedback matrix. The observer has to respond faster than the system with state feedback. Furthermore, the observer poles should not be too far in the left half plane since the observer would act as a differentiating system [1, 9]. Finally, the poles should have approximately the same distance from the origin.

A static state feedback $\mathbf{u} = -\mathbf{K_r}\,\mathbf{x}$ is chosen for control purposes. Using $\mathbf{u} \in R^q$ and $\mathbf{x} \in R^n$ the $(q\,\mathrm{x}\,n)$-feedback matrix $\mathbf{K_r}$ has $n \cdot q$ degrees of freedom. Equating the characteristic polynom with the target polynom,

$$\det\left[s\mathbf{I} - (\mathbf{A} - \mathbf{BK_r})\right] = \prod_{j=1}^{n}(s - s_j) \tag{45}$$

and comparing the coefficents, one obtains only n equations in spite of the $n \cdot q$ degrees of freedom. The further available degrees of freedom can be used for the fulfillment of further design targets, e.g. to reduce the control activity or to simplify the computation of the feedback matrix $\mathbf{K_r}$.

6.3.3 Pole Placement

The pole placement is done using the command 'place' in Matlab. For the controller, the poles are placed at one third of the value of the oberver's poles. The order of the multiple poles must not exceed the rank of the control matrix $\mathbf{B}$. Fig. 13 shows the transmissibility curves for the passive system, the loop shaping controller, and the pole placement controller cases. The system having the pole placement controller outperforms the passive system. However, the loop shaping controller performs better than the pole placement controller for the simulated excitation displacement. The performance of the loop shaping controller has to be further examined for the case of different excitations.

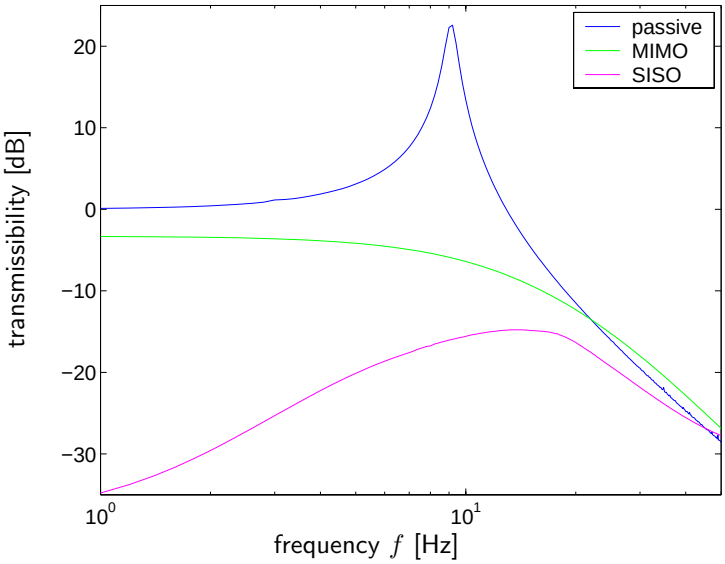

Figure 13: Simulated transmissibility curve of passive and active vibration isolation sytem with SISO and MIMO.

7 Conclusions

An active anti-vibration system has been investigated both theoretically and experimentally. Control performance demonstrates that the multichannel active isolation system can effectively reduce the vibration of the equipment structure over a wide frequency range. In future studies the three degree of freedom system model will be extended to a six degrees of freedom system so that active vibration control in horizontal directions needs to be implemented as well. A model-based control technique requires the accurate identification of model parameters. Therefore, it will also be necessary to develop an on-line parameter identification technique to cope with the influence which different loads have on the vibration isolation system. Furthermore, this research is restricted to excitation displacement. In future force excitation has also be considered. Finally, the control concepts have to be further developed, especially with respect to adaptive control algorithms and with respect to robust control.

References

[1] Föllinger, O.: Regelungstechnik. Hüttig Buch Verlag, Heidelberg, 1994.

[2] Fuller, C. R., Elliott, S. J., Nelson, P. A.: Active Control of Vibration. Academic Press, 1996.

[3] Ewins, D. J.: Modal Testing - Theory, Practice and Application. Research Studies Press LTD. Baldock, 2000.

[4] Huang, X., Elliott, S. J., Brennan, M. J.: Active isolation of a flexible structure from base vibration, Journal of Sound and Vibration, 263, 357–376, (2003).

[5] Hurlebaus, S.: Smart Structures - Fundamentals and Applications, Lectures Notes, Institute A of Mechanics, University of Stuttgart, 2004.

[6] Preumont, A.: Vibration Control of Active Structures. Kluwer Academic Publisher, Dordrecht, 1997.

[7] Preumont, A., Francois, A., Bossens, F. Abu-Hanieh, A.: Force feedback versus acceleration feedback in active vibration isolation. Journal of Sound and Vibration, 257(4), 605–613, (2002).

[8] Riebe, S., Ulbrich, H.: Modelling and online computation of the dynamics of a parallel kinematic with six degrees-of-freedom. Archive of Applied Mechanics, 72, 817–829, (2003).

[9] Schmid, W., Zeitz, M.: Grenzübergang Beobachter - Differenzierer. Regelungstechnik, 29, 270–274, (1981).

[10] Stöbener, U., Gaul, L.: Piezoelectric stack actuator: FE-modeling and application for vibration isolation. In: Proceedings of the NATO Advanced Study Institute on Responsive Systems for Active Vibration Control, Ed.: A. Preumont, Kluwer Academic Publishers, Dordrecht, 2001.